Relationship between exceptional points and the Kondo effect in f-electron materials

Yoshihiro Michishita,[1] Tsuneya Yoshida,[2] and Robert Peters[1]
[1]*Department of Physics, Kyoto University, Kyoto 606-8502, Japan*
[2]*Department of Physics, Tsukuba University, Tsukuba, Japan*

(Received 17 July 2019; revised manuscript received 30 January 2020; accepted 31 January 2020; published 14 February 2020)

We study the impact of non-Hermiticity due to strong correlations in f-electron materials. One of the most remarkable phenomena occurring in non-Hermitian systems is the emergence of exceptional points at which the effective non-Hermitian Hamiltonian cannot be diagonalized. We here demonstrate that the temperature at which exceptional points appear around the Fermi energy is related to the Kondo temperature. For this purpose, we study the periodic Anderson model with local and nonlocal hybridization in the insulating and metallic regimes. By analyzing the effective non-Hermitian Hamiltonian, which describes the single-particle spectral function, and the temperature dependence of the magnetic moment, we show that exceptional points appear at the temperature at which the magnetic moment is screened. This temperature corresponds to the Kondo temperature. These results suggest that the well-known crossover between localized and itinerant f electrons in these materials is related to the emergence of exceptional points in the single-particle spectral function at the Fermi energy. Viewing exceptional points in the combined momentum-frequency space, we observe that the exceptional points in the effective Hamiltonian form a one-dimensional manifold which changes its structure around the Kondo temperature.

DOI: 10.1103/PhysRevB.101.085122

I. INTRODUCTION

Recently, phenomena described by an effective non-Hermitian Hamiltonian have been intensively studied, especially in the context of artificial quantum systems [1–13]. An effective non-Hermitian Hamiltonian can induce novel topological phases [11,12,14–18] and novel phenomena such as anomalous edge states [7,15], unusual quantum critical phenomena [8,13,19], unidirectional invisibility [20–22], chiral transport [6,23–26], and enhanced sensitivity [9,27–32].

In open quantum systems, e.g., in cold atomic systems, it is possible to derive an effective non-Hermitian Hamiltonian under certain conditions even though the Hamiltonian describing the total system is Hermitian [33,34]. However, as the system becomes larger, it is difficult to experimentally realize these conditions, such as postselection or a $\mathcal{PT}$-symmetric setup. Thus, experiments about non-Hermitian phenomena in artificial quantum systems are particularly done in one-dimensional or small systems [6,26,30,31,35,36].

On the other hand, strongly correlated systems in equilibrium were not considered to be related to non-Hermitian systems until recently. Generally, the band structure of strongly correlated materials, which is given by the single-particle spectral function, is renormalized and broadened by the self-energy $\Sigma(\omega)$. The spectral function in equilibrium can always be written as $A(\omega) = -\frac{1}{\pi}\mathrm{Im}\{\mathrm{tr}(\omega - \mathcal{H}_{\mathrm{eff}})^{-1}\}$, where $\mathcal{H}_{\mathrm{eff}} = \mathcal{H}_0 + \Sigma$, $\mathcal{H}_0$ is the noninteracting part of the Hamiltonian, and Σ is the self-energy. The imaginary part of the self-energy can be related to the finite lifetime of the quasiparticles in the strongly correlated material. Until recently, the effect of the imaginary part of the self-energy was merely considered to be a broadening of the spectral function. However, Kozii and Fu [37] showed that because of the imaginary part of the self-energy, the effective Hamiltonian describing the spectral function is non-Hermitian, which can generate exotic phenomena [11,38,39]. For example, the effective non-Hermitian Hamiltonian can be defective at an exceptional point (EP) in the Brillouin zone (BZ), where it cannot be diagonalized. At these EPs, a topological number can be defined [11]. Moreover, different EPs in the BZ might be connected by bulk Fermi arcs which could be observed in angle-resolved photoemission spectroscopy (ARPES). These non-Hermitian phenomena, which can be seen in the equilibrium state of strongly correlated materials, are now studied vigorously. They also hold the potential to explain the pseudogap in cuprate superconductors or quantum oscillations in the topological Kondo insulators [38] SmB_6 [40,41] and YbB_{12} [42].

We note that to obtain an effective non-Hermitian Hamiltonian describing the spectral function, postselection or other difficult experimental setups are not necessary. Therefore, it seems reasonable that two-dimensional (2D) or three-dimensional (3D) bulk non-Hermitian phenomena can be more easily observed in strongly correlated materials than in artificial quantum systems.

It has been shown that the minimal model which can include exceptional points in the spectral function must consist of at least two hybridized bands, which include different self-energies. A model exactly describing this situation is the periodic Anderson model, which consists of an uncorrelated band which is hybridized with a strongly correlated band. This model is generally used to describe f-electron materials, where the uncorrelated band describes conduction (c) electrons and the correlated band describes f electrons. Because of the strong correlations, many remarkable phenomena can

be observed in f-electron materials, such as magnetism, unconventional superconductivity, quantum criticality, and the Kondo effect.

In this paper, we study non-Hermitian phenomena induced by the self-energy in the Kondo regime of 2D f-electron materials by using the dynamical mean-field theory (DMFT) [43] combined with the numerical renormalization group (NRG) [44–46]. We elucidate the relationship between the appearance of exceptional points (or exceptional loops) at the Fermi energy in the spectral function and the transition from a metal at high temperatures to the Kondo insulator or the heavy-fermion state at low temperature. Thus, the appearance of exceptional points at the Fermi energy corresponds to the transition from localized f electrons to itinerant f electrons [47–50]. We note that the emergence of exceptional points and bulk Fermi arcs has been reported in different versions of the periodic Anderson model [51] and the Kondo lattice model [39].

The rest of this paper is organized as follows. In Sec. II, we introduce the models, and we briefly explain exceptional points and the related non-Hermitian topological numbers in strongly correlated electron systems. In Sec. III, we show the numerical results by DMFT/NRG about the Kondo temperature and the temperature at which the exceptional points emerge at the Fermi surface. In Sec. IV, we analyze the structure of exceptional points in the combined momentum-frequency-space. In Sec. V, we conclude this paper.

II. MODELS AND NON-HERMITIAN PROPERTIES IN STRONGLY-CORRELATED ELECTRON SYSTEMS

To analyze the emergence of exceptional points and the Kondo effect in f-electron materials, we use the periodic Anderson model,

$$\mathcal{H} = \sum_{\boldsymbol{k}} [(\epsilon_{\boldsymbol{k}} + \mu_c) c^\dagger_{\boldsymbol{k}\sigma} c_{\boldsymbol{k}\sigma} + (\epsilon_{f\boldsymbol{k}} + \mu_f) f^\dagger_{\boldsymbol{k}\sigma} f_{\boldsymbol{k}\sigma} + (V_{l/p})_{\sigma\sigma'} (f^\dagger_{\boldsymbol{k}\sigma} c_{\boldsymbol{k}\sigma'} + \text{H.c.})] + U \sum_i n_{i\uparrow} n_{i\downarrow}, \quad (1a)$$

$$\epsilon_{c/f} = -2t_{c/f}(\cos k_x + \cos k_y) + \mu_{c/f}, \quad (1b)$$

$$V_l = V \delta_{\sigma\sigma'}, \quad (1c)$$

$$V_p = V(\boldsymbol{\sigma} \cdot \sin \boldsymbol{k}) \quad [\sin \boldsymbol{k} = (\sin k_x, \sin k_y)], \quad (1d)$$

$$n_{i\sigma} = f^\dagger_{i\sigma} f_{i\sigma}, \quad (1e)$$

where $c^{(\dagger)}_{\boldsymbol{k}\sigma}$ and $f^{(\dagger)}_{\boldsymbol{k}\sigma}$ are annihilation (creation) operators of the c and the f electrons for momentum $\boldsymbol{k}$ and spin direction σ. $t_{c,f}$ are the intersite hopping strengths for the c and the f electrons. For simplicity, we assume a two-dimensional square lattice. $\mu_{c/f}$ are the chemical potentials for the c and f orbitals. $V_{l/p}$ describe a local and a nonlocal hybridization between the c and f orbitals, respectively. Throughout this paper, we fix $t_f = \pm 0.05 t_c$, $\mu_c = 0$, $\mu_f = -1.0$, $U = 2.0$ and use $t_c = 0.8$. Using this model, we analyze the relation between the Kondo effect and the emergence of exceptional points. We will focus on three different cases: $t_f = -0.05 t_c$ with a local hybridization ($V_l \neq 0, V_p = 0$) in which the system becomes a Kondo insulator, $t_f = 0.05 t_c$ with a local hybridization ($V_l \neq 0, V_p = 0$) in which the system becomes a heavy metal, and $t_f = -0.05 t_c$ with a p-wave hybridization ($V_l = 0, V_p \neq 0$) in which the system becomes a heavy semimetal.

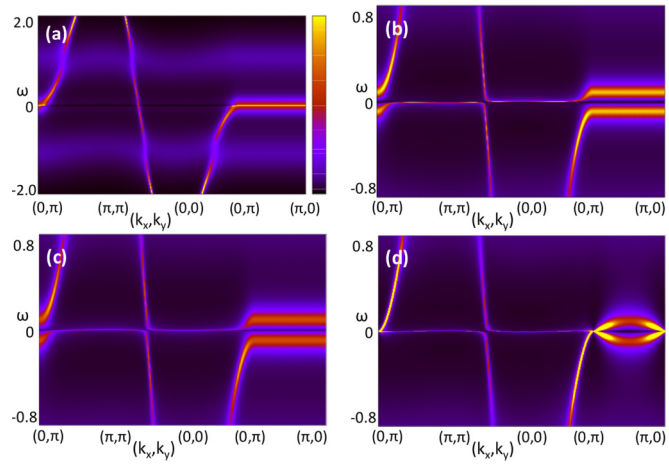

FIG. 1. Momentum-resolved spectral functions for the Kondo insulator, the heavy-fermion state, and the metallic state with p-wave hybridization for $V = 0.4$. (a) shows a high-temperature spectral function, $T = 0.13$ of the Kondo insulator. (b)–(d) show spectral functions at low temperatures, for $T = 0.0005$, for the Kondo insulator, the heavy-fermion state, and the nonlocal hybridization, respectively.

In Figs. 1 and 2, we show the momentum-resolved spectral functions and the Fermi surfaces for all three states. We use the self-energy which is calculated by the DMFT combined with NRG. DMFT takes local fluctuations fully into account by self-consistently solving the mean-field equations [43]. The lattice Hamiltonian is thereby mapped onto a quantum impurity model. DMFT neglects nonlocal fluctuations. Even though nonlocal fluctuations might not be small in 2D systems and might even be crucial for the magnetic state, they might be less important for the Kondo effect and the emergence of exceptional points. Furthermore, all shown results remain correct in three-dimensional systems, where nonlocal fluctuations are weaker compared to the 2D system. To solve

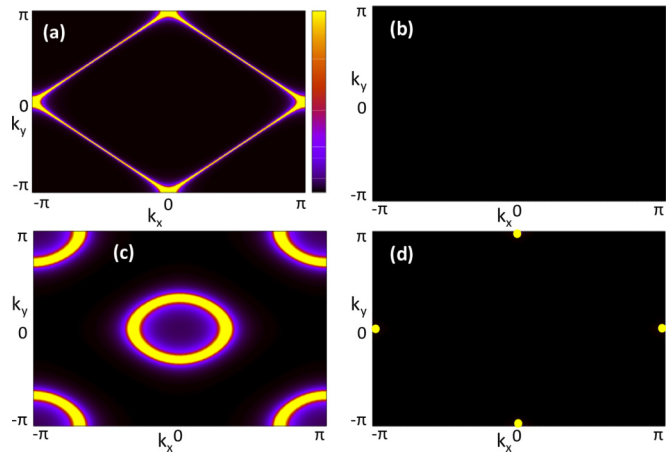

FIG. 2. Momentum-resolved spectral functions at $\omega = 0$ corresponding to the spectral functions shown in Fig. 1. In (d), we have enhanced the visibility of the Fermi surface by changing the color.

the quantum impurity model, we use the NRG, which calculates low-energy properties by iteratively discarding high-energy states. It has been shown that NRG is a very reliable tool at low temperature [45,46]. At high temperature, the f electrons are localized and do not hybridize with the c electrons, as shown in Figs. 1(a) and 2(a). Below the Kondo temperature, f electrons become itinerant and hybridize with the c electrons, which results in strong changes in the spectral function. Figure 1(b) shows the spectral function of the Kondo insulator having a gap at the Fermi energy. Figure 1(c) shows the spectral function of the metallic regime with local hybridization, and Fig. 1(d) shows the spectral function of the p-wave hybridization. Corresponding to these spectral functions, we show the spectral weight at the Fermi energy in Fig. 2. At high temperatures [Fig. 2(a)], we find only the c electrons at the Fermi energy. At low temperatures, all three states have very different Fermi surfaces. The Kondo insulating state, shown in Fig. 2(b), has no spectral weight at the Fermi energy. The heavy-Fermion state [Fig. 2(c)] shows the Fermi surface corresponding to a metallic state. Finally, in Fig. 2(d), the pointlike Fermi surface of the metallic state with p-wave hybridization is shown.

Before showing the main results, we briefly introduce exceptional points in strongly correlated materials. As mentioned above, the periodic Anderson model is a minimum model for the emergence of the exceptional points. The effective non-Hermitian Hamiltonian which describes the spectral function can be block diagonalized in the spin space and can be written by

$$\mathcal{H}_{\rm eff}(\boldsymbol{k},\omega)=\mathcal{H}_0+\Sigma(\omega)=\begin{pmatrix}\epsilon_c(\boldsymbol{k}) & V(\boldsymbol{k})\\ V(\boldsymbol{k}) & \epsilon_f(\boldsymbol{k})+\Sigma(\omega)\end{pmatrix}$$
$$=h_0\mathbf{1}+h_1\tau^z+V(\boldsymbol{k})\tau^x, \tag{2a}$$
$$h_0=[\epsilon_c(\boldsymbol{k})+\epsilon_f(\boldsymbol{k})+\Sigma(\omega)]/2, \tag{2b}$$
$$h_1=[\epsilon_c(\boldsymbol{k})-\epsilon_f(\boldsymbol{k})-\Sigma(\omega)]/2, \tag{2c}$$
$$E_\pm-h_0=\pm\sqrt{h_1^2+V^2(\boldsymbol{k})} \tag{2d}$$
$$=\pm\left\{\left(\frac{[\epsilon_c(\boldsymbol{k})-\epsilon_f(\boldsymbol{k})-{\rm Re}\Sigma(\omega)]^2}{4}+V^2(\boldsymbol{k})-\frac{[{\rm Im}\Sigma(\omega)]^2}{4}\right)+\frac{i}{2}({\rm Im}\Sigma(\omega)[\epsilon_c(\boldsymbol{k})-\epsilon_f(\boldsymbol{k})-{\rm Re}\Sigma(\omega)])\right\}^{\frac{1}{2}}, \tag{2e}$$

where $E_\pm$ are the eigenvalues of the effective Hamiltonian. τ^i corresponds to the Pauli matrices acting on the orbital indices. For the system with p-wave hybridization, we use the helical basis, in which $V(\boldsymbol{k})=V\sqrt{\sin^2(k_x)+\sin^2(k_y)}$. This effective non-Hermitian Hamiltonian becomes nondiagonalizable when the following conditions are satisfied:

$$\epsilon_c(\boldsymbol{k})-\epsilon_f(\boldsymbol{k})-{\rm Re}\Sigma(\omega)=0, \tag{3a}$$
$${\rm Im}\Sigma(\omega)/2=V(\boldsymbol{k}). \tag{3b}$$

These points (sometimes loops) in the momentum space, for which the non-Hermitian Hamiltonian cannot be diagonalized, are called exceptional points. Moreover, we can define a winding number on these points which reads [11]

$$W=\oint_{\rm EP}\frac{d\boldsymbol{k}}{2\pi i}\cdot\nabla_{\boldsymbol{k}}\ln\det\mathcal{H}_{\rm eff}(\boldsymbol{k},\omega). \tag{4}$$

Exceptional points with $W\neq 0$ are topologically stable because W does not change unless the exceptional point is annihilated by another one. We note that, in strongly correlated materials, the effective non-Hermitian Hamiltonian is introduced to describe the spectral function [39]. Therefore, when ${\rm Re}(\omega-h_0)$ is not small, the spectral weight at the exceptional points is small and might have only a small effect on observable phenomena. We will thus distinguish exceptional points with ${\rm Re}(\omega-h_0)\simeq 0$ from the exceptional points where $|{\rm Re}(\omega-h_0)|$ is large. In this paper, we call the former "exceptional points" and the latter "irrelevant exceptional points" (iEPs). In short, iEPs have less spectral weight and therefore are less relevant to physical phenomena than EPs. In this paper, we use the cutoff $|{\rm Re}(\omega-h_0)|<0.005$ to distinguish between EPs and iEPs.

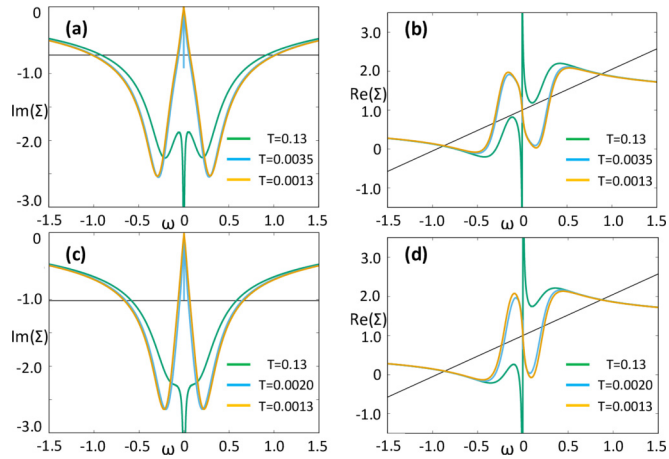

FIG. 3. The temperature dependence of the imaginary and real parts of the self-energy calculated by DMFT/NRG. (a) and (b) show the results for the local hybridization with $V=0.36$ and $t_f=-0.05t_c$. (c) and (d) show the results for the nonlocal hybridization with $V=0.36$ and $t_f=-0.05t_c$. The black lines in (a) and (c) describe the condition ${\rm Im}\Sigma(\omega)/2=\max|V(\boldsymbol{k})|$, and the black lines in (b) and (d) describe the conditions of Eq. (3a) and ${\rm Re}(\omega-h_0)=0$.

In Fig. 3, we show an example of the temperature dependence of the self-energy calculated by DMFT/NRG. The model with local hybridization, $V=0.36$, is shown in Figs. 3(a) and 3(b). Because Eq. (3b) is independent of the momentum for a system with local hybridization, Eq. (3b) can be satisfied for all $\boldsymbol{k}$ in the BZ, and therefore, EPs and iEPs can emerge at ω where the imaginary part of the self-energy crosses the black line. For the emergence of EPs which have strong spectral weight, additionally, ${\rm Re}(\omega-h_0)\simeq 0$ must be fulfilled. Because $(\epsilon_f-\mu_f)/(\epsilon_c-\mu_c)=$ const in our model, the momentum dependence vanishes for ${\rm Re}(\omega-h_0)=0$. Thus, the condition for the emergence of an EP can be written as $(\epsilon_c-\mu_c-\epsilon_f+\mu_f)\omega/(\epsilon_c-\mu_c)=\gamma\omega={\rm Re}\Sigma(\omega)+\mu_f$, where γ is a constant. In Figs. 3(b) and 3(d), this condition is fulfilled when the black line intersects with ${\rm Re}\Sigma(\omega)$. We note that even in a model where $(\epsilon_f-\mu_f)/(\epsilon_c-\mu_c)$ is not constant, the momentum dependence of ${\rm Re}(\omega-h_0)$ is small

because, usually, $(\epsilon_f - \mu_f)$ is much smaller than $(\epsilon_c - \mu_c)$. Thus, we see in Fig. 3 that the condition $\mathrm{Re}(w - h_0) = 0$ can be fulfilled at the Fermi energy.

For the system with nonlocal hybridization, shown in Figs. 3(c) and 3(d), Eq. (3b) can be satisfied at ω, where the absolute value of the imaginary part of the self-energy is smaller than the black line, because the strength of the hybridization depends on the momentum. Therefore, EPs and iEPs can appear more easily in this case, as we will show in the next section.

III. RELATION BETWEEN KONDO TEMPERATURE AND T_{EP} IN f-ELECTRON MATERIALS

Before showing the numerical results, let us consider the Kondo effect from the non-Hermitian point of view in a two-orbital periodic Anderson model. The imaginary part of the self-energy plays here an essential role to create non-Hermitian effects. At high temperature, the imaginary part of the self-energy has a peak at $\omega = 0$, and $\mathrm{Im}\Sigma \gg V$ is satisfied around the Fermi energy. Equation (2d) is given in the first order of $V/\mathrm{Im}\Sigma$ as

$$E_{\pm} = h_0 \mp \frac{i\mathrm{Im}\Sigma}{2}\left(1 + \frac{4\mathrm{Re}h_1}{i\mathrm{Im}\Sigma} - \frac{4(V^2 + (\mathrm{Re}h_1)^2)}{(\mathrm{Im}\Sigma)^2}\right)^{\frac{1}{2}} \tag{5a}$$

$$\simeq h_0 \mp \frac{i\mathrm{Im}\Sigma}{2}\left(1 + \frac{2\mathrm{Re}h_1}{i\mathrm{Im}\Sigma}\right) = \epsilon_c, \epsilon_f + \Sigma, \tag{5b}$$

which shows that f electrons are localized. On the other hand, below the Kondo temperature, the imaginary part of the self-energy becomes small, satisfying $\mathrm{Im}\Sigma \ll V$, and therefore, the eigenvalues of the effective non-Hermitian Hamiltonian become $E_{\pm} = \mathrm{Re}(h_0) \pm \sqrt{\mathrm{Re}(h_1)^2 + V^2}$, which show that f electrons are hybridized and become itinerant. Thus, during the crossover from localized to itinerant f electrons, the self-energy satisfies $\mathrm{Im}\Sigma \sim V$, and the condition for the emergence of exceptional points in Eq. (3b) is fulfilled. In this paper, we assume that there is no magnetically ordered phase. This assumption is justified because there are many f-electron materials, such as $Ce_3Bi_4Pt_3$ [52,53], SmB_6 [54], and YbB_{12} [55], in which the Kondo crossover occurs in the magnetically disordered phase. Furthermore, the tendency towards magnetically ordered phases is suppressed at strong hybridization strengths, so that it is justified to assume that the Kondo effect occurs in the magnetically disordered phase. Therefore, we can anticipate the emergence of exceptional points at the Fermi energy around the Kondo temperature. In a periodic Anderson model including more orbitals, exceptional points due to hybridization between different orbitals can occur, and a more detailed analysis is necessary.

In Figs. 4(a)–4(c), we show the magnetic moment of the f electrons [contribution of the f electron to the magnetic susceptibility $T\chi_f^z(T)$]. Around the Kondo temperature, the magnetic moment changes from 0.25 at high temperatures to zero at low temperatures, which corresponds to the Kondo screening. The magnetic susceptibility in Figs. 4(a)–4(c) is thereby calculated by applying a tiny magnetic field to the system and calculating the induced magnetic polarization of the f electrons. We here estimate the Kondo temperature as the temperature at which the magnetic moment crosses $T\chi = 0.125$ in Figs. 4(a)–4(c) and include an arrow at these temperatures. We note that this screening is a crossover occurring over a finite-temperature range. Thus, the Kondo temperature can also be determined only approximately within the temperature region where the magnetic moment is screened. For the metallic system with local hybridization shown in Fig. 4(b), the screening occurs more slowly than in the other cases. In this system, the Fermi surface does not vanish below the Kondo temperature, so that scattering around the Fermi surface can occur, and the imaginary part of the self-energy at the Fermi energy decreases only slowly with lowering the temperature. Although the system with nonlocal hybridization shown in Figs. 4(c) and 4(f) also has a Fermi surface, it is almost pointlike, and therefore, it induces much less scattering, resulting in a fast screening.

In addition to analyzing the Kondo screening, we can use the self-energies obtained by DMFT/NRG to analyze the emergence of EPs in the spectrum and the temperature at which the EPs appear at the Fermi energy. We show these EPs in Figs. 4(g)–4(i), where we plot iEPs with large eigenvalue $\mathrm{Re}(\omega - h_0)$ as black dots and EPs with $\mathrm{Re}(\omega - h_0) \simeq 0$ as colored squares corresponding to the colors of the hybridization shown in Figs. 4(a)–4(c). We see that EPs with $\mathrm{Re}(\omega - h_0) \simeq 0$ appear only in a narrow temperature region for the system with the local hybridization and below a certain temperature for the system with nonlocal hybridization. In Fig. 4(e), EPs appear in a wider temperature range than in Fig. 4(d) because the self-energy changes only slowly when lowering the temperature. Finally, in Fig. 4(f), EPs can emerge below a certain temperature because of the momentum dependence of the hybridization, which makes it easier to satisfy Eq. (3b). Furthermore, in Fig. 4(f), EPs appear also far from $\omega = 0$. This is possible because, for the system with the nonlocal hybridization, the conditions for the emergence of EPs can be satisfied more easily. However, the emergence of EPs far from $\omega = 0$ seems to be irrelevant to the Kondo effect because the Kondo effect stems from the scattering around the Fermi surface.

Comparing the temperature at which EPs with $\mathrm{Re}(\omega - h_0) \simeq 0$ appear and the temperature at which the magnetic moment of the f electron is screened, we see that both temperatures match very well. Thus, we conclude that the Kondo temperature is closely related to the temperature where EPs emerge at the Fermi energy. When lowering the temperature, the self-energy at the Fermi energy changes very strongly around the Kondo temperature, which results in a situation in which Eqs. (3a) and (3b) can be easily fulfilled at the Fermi energy. For the system with the p-wave hybridization, the EPs start to emerge at the Kondo temperature when the absolute value of the imaginary part of the self-energy becomes smaller than the hybridization strength.

In Figs. 4(d)–4(f), we can also see many iEPs with large $\mathrm{Re}(\omega - h_0)$, which appear at almost all temperatures. These iEPs are mainly related to the imaginary part of the self-energy away from the Fermi energy, particularly in the Hubbard bands, which are nearly temperature independent and are irrelevant to the Kondo effect.

Figures 4(g)–4(i) show the Fermi surface at the temperature at which EPs appear at the Fermi energy for the systems

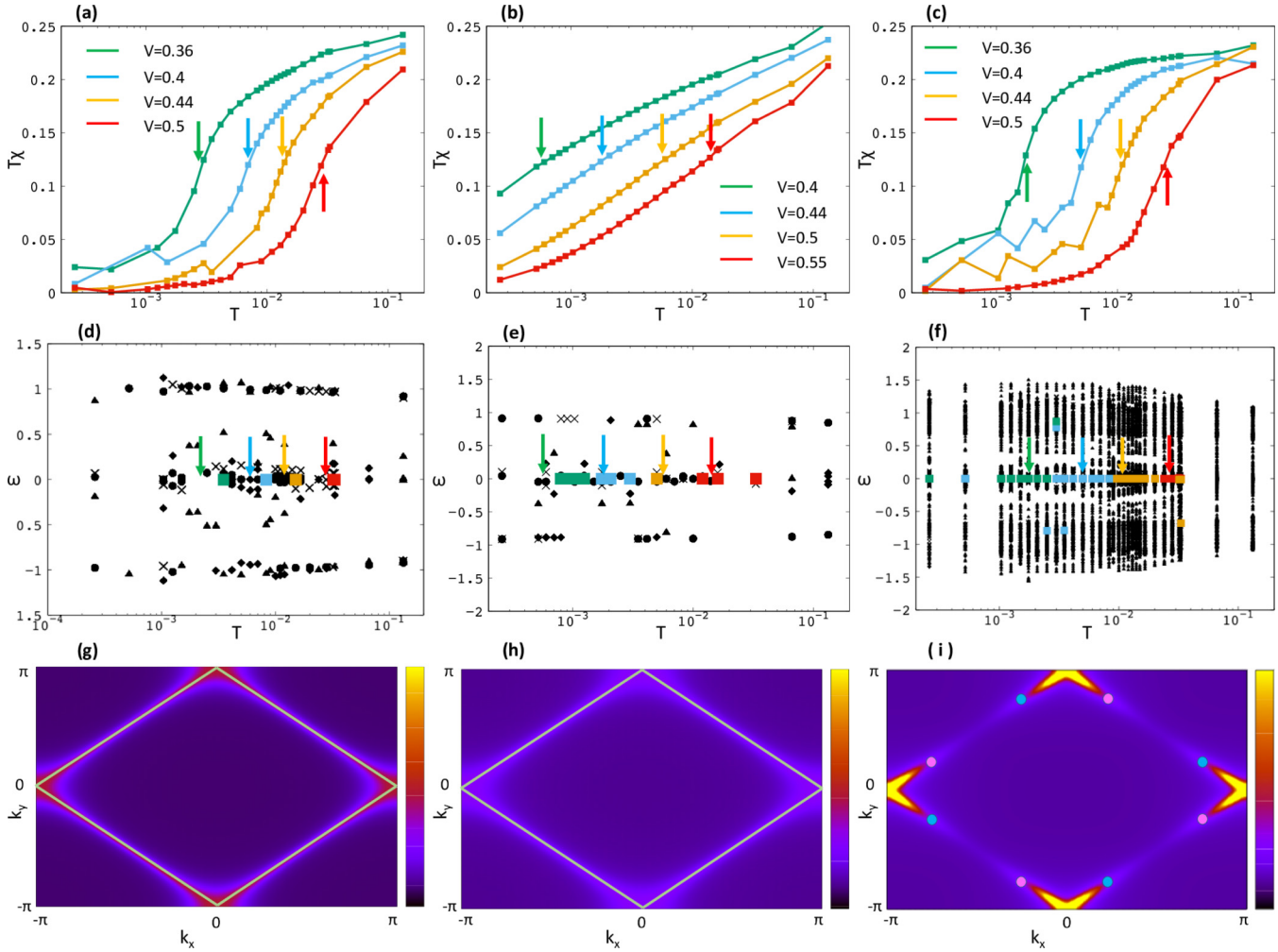

FIG. 4. (a)–(f) Comparison between the Kondo insulator, the heavy-fermion state, and the metallic state with p-wave hybridization for different strengths of V. (a)–(c) show the local susceptibility. The colors in (a)–(c) correspond to different V. The arrows describe the estimated Kondo temperature for each case. In (a) and (c), green, sky blue, orange, and red lines respectively correspond to $V = 0.36, 0.4, 0.44, 0.5$. In (b), the green, sky blue, orange, and red lines respectively correspond to $V = 0.4, 0.44, 0.5, 0.55$. (d)–(f) show the temperature and the frequency dependence of the emergence of the iEPs and the EPs. The iEPs are drawn as black dots. In (d) and (f), the crosses, points, triangles, and squares are for $V = 0.36, 0.4, 0.44, 0.5$. In (e), the crosses, points, triangles, and squares correspond to $V = 0.4, 0.44, 0.5, 0.55$. The EPs are drawn as color plots. We use the same color as in (a)–(c). The arrows describe the Kondo temperature estimated from (a)–(c). We use the cutoff $|\mathrm{Re}(\omega - h_0)| < 0.005$, which distinguishes between EPs and iEPs. If $|\omega - \mathrm{Re}h_0| < 0.005$, we call them EPs; otherwise, we call them iEPs. (g)–(i) show momentum-resolved spectral functions at the Fermi energy around T_{EP}. (g) corresponds to $V = 0.36$, $T = 0.0035$ shown in (a) and (d). (h) corresponds to $V = 0.4$, $T = 0.0007$ shown in (b) and (e). (i) corresponds to $V = 0.36$, $T = 0.0025$ shown in (c) and (f). The parameters are $U = 2$, $t_c = 0.8$, $t_f = -0.04$, $\mu_c = 0$, $\mu_f = -1.0$. In (g) and (h), exceptional points form a closed loop in the BZ, highlighted as a green line. In (i), we included exceptional points with vorticity $\pm 1/2$ as red and blue points.

with local hybridization and for the system with p-wave hybridization. For the system with the local hybridization, EPs appear only at T_{EP} and form a closed loop in the BZ. We note that it is not possible to define a vorticity at $\omega = 0$ for this closed loop, which is different from the symmetry-protected exceptional ring in systems with chiral symmetry [56–59]. Therefore, we believe that this loop of exceptional points will change into isolated EPs connected by bulk Fermi arcs when taking into account a momentum-dependent self-energy. For the system with the p-wave hybridization, EPs appear as isolated points at the Fermi energy in the spectrum and have nonzero vorticity and are thus topologically protected. These EPs change their position in the BZ satisfying Eq. (3a) with changing temperature and finally merge and disappear at zero temperature.

IV. EXTENSION OF THE EXCEPTIONAL MANIFOLDS TO ω SPACE

For the emergence of exceptional points, two equations [Eqs. (3a) and (3b)] must be satisfied. Thus, in a d-dimensional model (two-dimensional momentum space in this paper), exceptional points will generally form $(d-2)$-dimensional manifolds. The dimension of the exceptional manifold might be higher if additional symmetries do exist. For example, in 2D systems with chiral symmetry [58], one

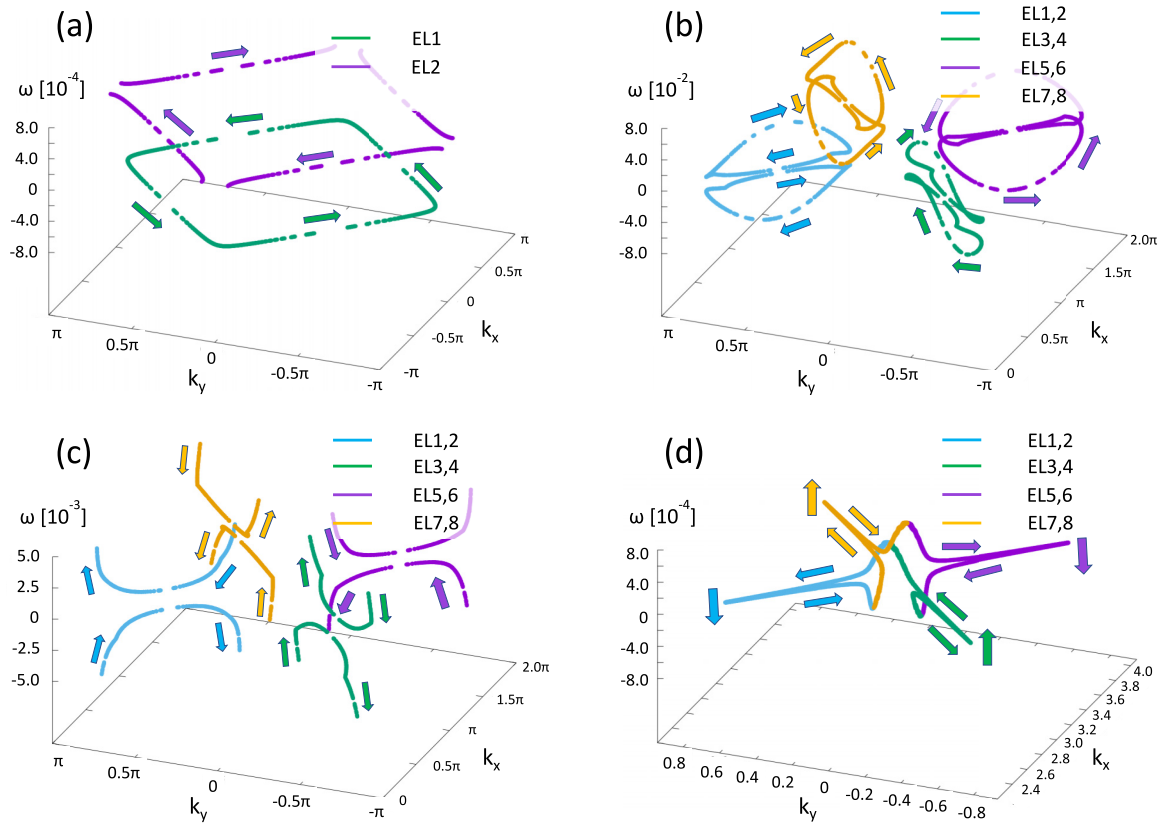

FIG. 5. Exceptional points of $\mathcal{H}_{\rm eff}(k_x, k_y, \omega)$ in the system (a) with local hybridization and (b)–(d) with nonlocal hybridization. The parameters are $V_l = 0.4$, $t_f/t_c = -0.05$, $T = 0.016$ in (a), $V_p = 0.4$, $t_f/t_c = -0.05$, $T = 0.016$ in (b) and (c), and $V_l = 0.4$, $t_f/t_c = -0.05$, $T = 0.002$ in (d). (c) is a magnification of the exceptional manifold shown in (b) close to the Fermi energy. The arrows in (a)–(d) describe the tangent vectors of exceptional manifolds. We choose the direction of the tangent vector so that the vorticity defined by Eq. (6) becomes $1/2$.

of the two conditions for EPs, such as Eqs. (3a) and (3b), is always satisfied, which leads to $(d-1)$-dimensional exceptional manifolds.

Besides the spatial dimension, the effective Hamiltonian in strongly correlated systems also depends on the frequency ω because the self-energy depends on the frequency. Thus, the inclusion of frequency will increase the dimension of the exceptional manifolds. Previous studies have focused on only the Fermi energy, ignoring the frequency dependence of the exceptional manifolds. We note that a frequency-dependent effective Hamiltonian occurs in situations when focusing on a subsystem and integrating out the rest of the total system, even though the full system is described by a frequency-independent Hamiltonian [60–62]. Because we here focus on the one-particle Green function, the effective Hamiltonian depends on the frequency.

In Fig. 5, we show the exceptional manifolds for the local and nonlocal hybridizations and different temperatures in the $(\boldsymbol{k}, \omega)$ space. Until now, we have focused only on exceptional points close to the Fermi energy. Figure 5(a) shows the exceptional loops in the system with local hybridization for a temperature above the Kondo temperature. As described above, in the system with local hybridization, Eqs. (3a) and (3b) do not depend on the momentum, and thus, exceptional manifolds are loops in the momentum space. At temperatures above the Kondo temperature, we find one loop above the Fermi energy and one loop below the Fermi energy. Lowering the temperature towards the Kondo temperature, these exceptional loops move towards the Fermi energy. At the Kondo temperature, these exceptional loops merge at the Fermi energy.

We note that by extending our considerations to the $(\boldsymbol{k}, \omega)$ space, we are able to define and calculate the vorticity of these loops by

$$\nu = \oint_{\rm EP} \frac{d\boldsymbol{k}'}{2\pi i} \cdot \nabla_{\boldsymbol{k}'} \log \det \mathcal{H}_{\rm eff}(\boldsymbol{k}, \omega), \tag{6}$$

where $\boldsymbol{k}'$ is defined on the plane which is perpendicular to the tangent vector of the exceptional loop. The line integral is done in the mathematical positive direction. We then define the direction of the exceptional loops, shown in Fig. 5, so that the vorticities defined in Eq. (6) become $1/2$. Further details are explained in the Appendix. We note that when considering a momentum-dependent self-energy, these loops become distorted. Thus, looking at the Fermi energy, the exceptional manifold will appear as points.

Figures 5(b)–5(d) show the exceptional manifolds for the system with nonlocal hybridization. Because Eqs. (3a) and (3b) depend on the momentum for a nonlocal hybridization, the exceptional manifolds are points in the momentum space for fixed ω. Figures 5(b) and 5(c) show these exceptional points in $(\boldsymbol{k}, \omega)$ space at high temperatures. Including the ω space, these exceptional points form closed loops.

Furthermore, we show in Fig. 5(c) a magnification of Fig. 5(b) around the Fermi energy, which demonstrates the absence of exceptional points at the Fermi energy for high temperatures. When lowering the temperature, one closed loop of EPs is formed above $\omega = 0$, and one closed loop is formed below $\omega = 0$. At the Kondo temperature, these loops touch and merge at $\omega = 0$ to a single one-dimensional exceptional manifold, as shown in Fig. 5(d).

We conclude that the crossover from localized to itinerant f electrons in the system with local hybridization goes hand in hand with the merging and vanishing of two exceptional loops at the Fermi energy. In the system with nonlocal hybridization, different exceptional loops in the $(\boldsymbol{k}, \omega)$ space change their topology at the Kondo temperature and generate EPs at the Fermi energy. Although the shape of the peak in the imaginary part of the self-energy at the Fermi energy might depend on the details of the model, the imaginary part of the self-energy must have the peak at $\omega \sim 0$ at high temperature and continuously decreases to zero around the Kondo temperature with decreasing temperature. Thus, the conditions for the emergence of exceptional points at the Fermi energy will be fulfilled at some temperature around the Kondo temperature independent of the exact shape of the peak in the imaginary part of the self-energy.

V. CONCLUSION AND DISCUSSION

In summary, we have shown a relation between the Kondo temperature and the emergence of exceptional points at the Fermi energy in f-electron materials. Particularly, we have studied the Kondo insulator and the metallic state with a local hybridization and the semimetallic state with a p-wave hybridization in the 2D periodic Anderson model by DMFT/NRG. Around the Kondo temperature, f electrons change from localized to itinerant when lowering the temperature. Thus, the emergence of EPs at the Fermi surface is a sign of the crossover between localized and itinerant f electrons. The emergence of EPs is a robust feature in a periodic Anderson model, for which the energy dispersions of the f-electron band and the c-electron band intersect at the Fermi energy and where the f electrons change from localized at high temperatures to itinerant (hybridized) at low temperature. We have also shown that the exceptional manifolds have a structure one dimension higher when considering the ω dependence of the effective Hamiltonian. For the system with the local hybridization, there are exceptional loops above and below $\omega = 0$ in the $(\boldsymbol{k}, \omega)$ space at high temperature, which merge and disappear around the Kondo temperature. For the p-wave hybridization, there are four exceptional loops each above and below $\omega = 0$ in the $(\boldsymbol{k}, \omega)$ space at high temperature, which merge and change their topology around the Kondo temperature. Contrary to the system with local hybridization, these exceptional manifolds at the Fermi energy are stable for a wide range of temperatures below the Kondo temperature, and these EPs are connected by bulk Fermi arcs.

In this paper, we have not considered the momentum dependence of the self-energy. However, even if the self-energy has a momentum dependence, the imaginary part of the self-energy at the Fermi energy must change from a large value at high temperatures to zero at low temperatures, corresponding to the crossover between localized and itinerant f electrons. At some temperature during this crossover, the conditions for the emergence of exceptional points Eq. (3a) and (3b) are fulfilled. Equation (3a) is satisfied at some momenta at the Fermi energy whenever the c- and f-electron bands are partially filled and both bands intersect at the Fermi energy. Equation (3b) must be satisfied at some temperature because the imaginary part of the self-energy smoothly changes from large values at high temperatures to zero at low temperatures. Thus, our conclusions about the emergence of EPs at the Fermi energy is unchanged when taking the momentum dependence of the self-energy into account. We note, however, that a momentum-dependent self-energy will deform exceptional loops in the $(\boldsymbol{k}, \omega)$ space. We believe that exceptional points are detectable via ARPES by direct observation of the Fermi arcs, which connect two EPs, or by tunneling experiments which might detect an increased density of states due to the EPs.

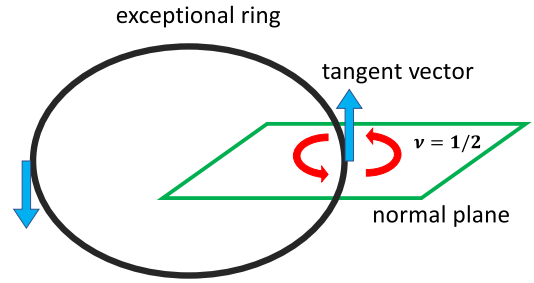

FIG. 6. Visualization of the tangent vector, normal plane, and the vorticity.

We can naturally expect that the relation between the emergence of exceptional points at the Fermi energy and the Kondo temperature holds for three-dimensional systems because the DMFT results become more accurate for higher dimensions. Because the band structure of the 3D system can be understood by stacking 2D systems, the 3D f-electron material should host robust exceptional rings in the case of a momentum-dependent hybridization and exceptional surfaces in the case of a local hybridization at the Fermi energy.

ACKNOWLEDGMENTS

This work is partly supported by JSPS KAKENHI Grants No. JP18H04316, No. JP18H05842, No. JP18K03511, and JP19K21032. Computer simulations were performed on the supercomputer of the Institute for Solid State Physics in the University of Tokyo.

APPENDIX: DEFINITION OF THE VORTICITY IN $(\boldsymbol{k}, \omega)$ SPACE

Here, we explain the details of the definition of the vorticity in the $(\boldsymbol{k}, \omega)$ space. In $(2+1)$-dimensional systems, exceptional points form a loop in the $(\boldsymbol{k}, \omega)$ space. In order to define the vorticity of the exceptional loop, we set up the plane in the $(\boldsymbol{k}, \omega)$ space to which the tangent vector of the loop is the normal vector (see Fig. 6). We calculate the vorticity by doing the following line integral in the mathematical positive

direction:

$$\nu = \oint_{\mathrm{EP}} \frac{d\boldsymbol{k}'}{2\pi i} \cdot \nabla_{\boldsymbol{k}'} \log \det \mathcal{H}_{\mathrm{eff}}(\boldsymbol{k}, \omega), \tag{A1}$$

where $\boldsymbol{k}'$ is defined on the plane, as shown in Fig. 6.

However, the sign of the integral still depends on the orientation of the plane, which depends on the direction of the tangent vector. Therefore, we choose the direction of the tangent vector so that the integral in Eq. (A1) becomes 1/2. This uniquely defines a direction for the exceptional loop in the $(\boldsymbol{k}, \omega)$ space, which is shown in Fig. 5. To define the vorticity in this way, we need to define a plane perpendicular to the exceptional manifold. Thus, it is necessary that the dimension of the exceptional manifold is $(d-2)$, where d is the dimension of the $(\boldsymbol{k}, \omega)$ space. By using Eqs. (3a) and (3b), we see that exceptional points can merge and disappear only if their tangent vectors are antiparallel, when two loops touch. We note that in systems whose Hamiltonian is described by a matrix larger than 2 by 2, e.g., a system including more than two orbitals, exceptional points generated by different pairs of eigenvalues can touch with arbitrary direction without merging. Furthermore, we note that a similar definition might be used to analyze two-dimensional exceptional manifolds in $(3+1)$-dimensional systems.

[1] N. Hatano and D. R. Nelson, Phys. Rev. Lett. **77**, 570 (1996).
[2] N. Hatano and D. R. Nelson, Phys. Rev. B **56**, 8651 (1997).
[3] M. Liertzer, L. Ge, A. Cerjan, A. D. Stone, H. E. Türeci, and S. Rotter, Phys. Rev. Lett. **108**, 173901 (2012).
[4] M. Brandstetter, M. Liertzer, C. Deutsch, P. Klang, J. Schöberl, H. Türeci, G. Strasser, K. Unterrainer, and S. Rotter, Nat. Commun. **5**, 4034 (2014).
[5] P. San-Jose, J. Cayao, E. Prada, and R. Aguado, Sci. Rep. **6**, 21427 (2016).
[6] J. Doppler, A. A. Mailybaev, J. Böhm, U. Kuhl, A. Girschik, F. Libisch, T. J. Milburn, P. Rabl, N. Moiseyev, and S. Rotter, Nature (London) **537**, 76 (2016).
[7] T. E. Lee, Phys. Rev. Lett. **116**, 133903 (2016).
[8] Y. Ashida, S. Furukawa, and M. Ueda, Nat. Commun. **8**, 15791 (2017).
[9] W. Chen, Ş. K. Özdemir, G. Zhao, J. Wiersig, and L. Yang, Nature (London) **548**, 192 (2017).
[10] L. Feng, R. El-Ganainy, and L. Ge, Nat. Photonics **11**, 752 (2017).
[11] H. Shen, B. Zhen, and L. Fu, Phys. Rev. Lett. **120**, 146402 (2018).
[12] Z. Gong, Y. Ashida, K. Kawabata, K. Takasan, S. Higashikawa, and M. Ueda, Phys. Rev. X **8**, 031079 (2018).
[13] M. Nakagawa, N. Kawakami, and M. Ueda, Phys. Rev. Lett. **121**, 203001 (2018).
[14] F. K. Kunst, E. Edvardsson, J. C. Budich, and E. J. Bergholtz, Phys. Rev. Lett. **121**, 026808 (2018).
[15] S. Yao and Z. Wang, Phys. Rev. Lett. **121**, 086803 (2018).
[16] S. Yao, F. Song, and Z. Wang, Phys. Rev. Lett. **121**, 136802 (2018).
[17] K. Kawabata, K. Shiozaki, M. Ueda, and M. Sato, Phys. Rev. X**9**, 041015 (2019).
[18] K. Kawabata, S. Higashikawa, Z. Gong, Y. Ashida, and M. Ueda, Nat. Commun. **10**, 297 (2019).
[19] K. Yamamoto, M. Nakagawa, K. Adachi, K. Takasan, M. Ueda, and N. Kawakami, Phys. Rev. Lett.**123**, 123601 (2019).
[20] Z. Lin, H. Ramezani, T. Eichelkraut, T. Kottos, H. Cao, and D. N. Christodoulides, Phys. Rev. Lett. **106**, 213901 (2011).
[21] A. Regensburger, C. Bersch, M.-A. Miri, G. Onishchukov, D. N. Christodoulides, and U. Peschel, Nature (London) **488**, 167 (2012).
[22] L. Feng, Z. J. Wong, R.-M. Ma, Y. Wang, and X. Zhang, Science **346**, 972 (2014).
[23] C. Dembowski, H.-D. Gräf, H. L. Harney, A. Heine, W. D. Heiss, H. Rehfeld, and A. Richter, Phys. Rev. Lett. **86**, 787 (2001).
[24] B. Peng, Ş. K. Özdemir, F. Lei, F. Monifi, M. Gianfreda, G. L. Long, S. Fan, F. Nori, C. M. Bender, and L. Yang, Nat. Phys. **10**, 394 (2014).
[25] T. Gao, E. Estrecho, K. Bliokh, T. Liew, M. Fraser, S. Brodbeck, M. Kamp, C. Schneider, S. Höfling, Y. Yamamoto *et al.*, Nature (London) **526**, 554 (2015).
[26] H. Xu, D. Mason, L. Jiang, and J. Harris, Nature (London) **537**, 80 (2016).
[27] T. E. Lee and C.-K. Chan, Phys. Rev. X **4**, 041001 (2014).
[28] J. Wiersig, Phys. Rev. Lett. **112**, 203901 (2014).
[29] Z.-P. Liu, J. Zhang, Ş. K. Özdemir, B. Peng, H. Jing, X.-Y. Lü, C.-W. Li, L. Yang, F. Nori, and Y.-x. Liu, Phys. Rev. Lett. **117**, 110802 (2016).
[30] H. Hodaei, A. U. Hassan, S. Wittek, H. Garcia-Gracia, R. El-Ganainy, D. N. Christodoulides, and M. Khajavikhan, Nature (London) **548**, 187 (2017).
[31] J. W. Yoon, Y. Choi, C. Hahn, G. Kim, S. H. Song, K.-Y. Yang, J. Y. Lee, Y. Kim, C. S. Lee, J. K. Shin *et al.*, Nature (London) **562**, 86 (2018).
[32] H.-K. Lau and A. A. Clerk, Nat. Commun. **9**, 4320 (2018).
[33] F. Reiter and A. S. Sørensen, Phys. Rev. A **85**, 032111 (2012).
[34] Y. Ashida, S. Furukawa, and M. Ueda, Phys. Rev. A **94**, 053615 (2016).
[35] A. Guo, G. J. Salamo, D. Duchesne, R. Morandotti, M. Volatier-Ravat, V. Aimez, G. A. Siviloglou, and D. N. Christodoulides, Phys. Rev. Lett. **103**, 093902 (2009).
[36] C. E. Rüter, K. G. Makris, R. El-Ganainy, D. N. Christodoulides, M. Segev, and D. Kip, Nat. Phys. **6**, 192 (2010).
[37] V. Kozii and L. Fu, arXiv:1708.05841.
[38] H. Shen and L. Fu, Phys. Rev. Lett. **121**, 026403 (2018).
[39] T. Yoshida, R. Peters, and N. Kawakami, Phys. Rev. B **98**, 035141 (2018).
[40] B. S. Tan, Y.-T. Hsu, B. Zeng, M. C. Hatnean, N. Harrison, Z. Zhu, M. Hartstein, M. Kiourlappou, A. Srivastava, M. D. Johannes *et al.*, Science **349**, 287 (2015).
[41] H. Liu, M. Hartstein, G. J. Wallace, A. J. Davies, M. C. Hatnean, M. D. Johannes, N. Shitsevalova, G. Balakrishnan, and S. E. Sebastian, J. Phys.: Condens. Matter **30**, 16LT01 (2018).
[42] Z. Xiang, Y. Kasahara, T. Asaba, B. Lawson, C. Tinsman, L. Chen, K. Sugimoto, S. Kawaguchi, Y. Sato, G. Li *et al.*, Science **362**, 65 (2018).
[43] A. Georges, G. Kotliar, W. Krauth, and M. J. Rozenberg, Rev. Mod. Phys. **68**, 13 (1996).
[44] K. G. Wilson, Rev. Mod. Phys. **47**, 773 (1975).

[45] R. Bulla, T. A. Costi, and T. Pruschke, Rev. Mod. Phys. **80**, 395 (2008).
[46] R. Peters, T. Pruschke, and F. B. Anders, Phys. Rev. B **74**, 245114 (2006).
[47] J. H. Shim, K. Haule, and G. Kotliar, Science **318**, 1615 (2007).
[48] O. Bodensiek, R. Žitko, R. Peters, and T. Pruschke, J. Phys.: Condens. Matter **23**, 094212 (2011).
[49] A. Benlagra, T. Pruschke, and M. Vojta, Phys. Rev. B **84**, 195141 (2011).
[50] R. Peters and N. Kawakami, Phys. Rev. B **92**, 075103 (2015).
[51] Y. Nagai, Y. Qi, H. Isobe, V. Kozii, and L. Fu (unpublished).
[52] M. F. Hundley, P. C. Canfield, J. D. Thompson, Z. Fisk, and J. M. Lawrence, Phys. Rev. B **42**, 6842 (1990).
[53] A. Severing, J. D. Thompson, P. C. Canfield, Z. Fisk, and P. Riseborough, Phys. Rev. B **44**, 6832 (1991).
[54] A. Menth, E. Buehler, and T. H. Geballe, Phys. Rev. Lett. **22**, 295 (1969).
[55] M. Kasaya, F. Iga, K. Negishi, S. Nakai, and T. Kasuya, J. Magn. Magn. Mater. **31–34**, 437 (1983).
[56] J. C. Budich, J. Carlström, F. K. Kunst, and E. J. Bergholtz, Phys. Rev. B **99**, 041406(R) (2019).
[57] R. Okugawa and T. Yokoyama, Phys. Rev. B **99**, 041202(R) (2019).
[58] T. Yoshida, R. Peters, N. Kawakami, and Y. Hatsugai, Phys. Rev. B **99**, 121101(R) (2019).
[59] T. Yoshida and Y. Hatsugai, Phys. Rev. B **100**, 054109 (2019).
[60] H. Feshbach, Ann. Phys. (NY) **5**, 357 (1958).
[61] H. Feshbach, Ann. Phys. (NY) **19**, 287 (1962).
[62] H.-P. Breuer and F. Petruccione, *The Theory of Open Quantum Systems* (Oxford University Press, Oxford, 2002).